Advances in Geo-Energy Research

Vol. 19, No. 3, p. 250-267, 2026

Original article

Mechanical responses and fracture behaviors of pre-heat-treated carbonate rocks during hydraulic fracturing under different confining-axial pressures

Peng Li[1]*, Chenyu Tang[1], Xinghui Wu[1,2]*, Yan Liu[1], Meifeng Cai[1], Mostafa Gorjian[3]

[1]*Beijing Key Laboratory of Urban Underground Space Engineering, University of Science and Technology Beijing, Beijing 100083, P. R. China*

[2]*School of City and Architecture Engineering, Zaozhuang University, Zaozhuang 277160, P. R. China*

[3]*Department of Earth, Ocean and Atmospheric Sciences, University of British Columbia, Vancouver, BC, V6T 1Z4, Canada*

Keywords:
Carbonate rocks
hydraulic fracturing
fracture morphology
fracture behaviors
failure modes

Cited as:
Li, P., Tang, C., Wu, X., Liu, Y., Cai, M., Gorjian, M. Mechanical responses and fracture behaviors of pre-heat-treated carbonate rocks during hydraulic fracturing under different confining-axial pressures. Advances in Geo-Energy Research, 2026, 19(3): 250-267.
https://doi.org/10.46690/ager.2026.03.05

Abstract:
In this work, the mechanical responses and fracture behaviors of pre-heat-treated carbonate rocks during hydraulic fracturing under different confining-axial pressure conditions were systematically investigated. Hydraulic fracturing tests were conducted on carbonate rock samples from the Gaoyuzhuang Formation in Xiongan New Area, China, under equal confining-axial pressures following various temperature pre-treatments. By integrating fluid pressure monitoring, acoustic emission signal acquisition, and three-dimensional fracture morphology scanning, the coupled effects of pre-treatment temperature and stress on fracture pressure, fracture propagation paths, and failure modes were systematically analyzed. The results demonstrate that pre-treatment temperature exerts a significant non-monotonic regulatory effect on rock mechanical behavior. Moderate-low temperatures enhance rock structural integrity, increasing both fracture pressure and the fluid pressure growth rate. In contrast, high temperatures induce micro-fracture networks through thermal stress, resulting in material weakening. Increasing confining-axial pressure not only significantly elevates fracture pressure but also suppresses thermal crack propagation, promoting a transition in failure mode from tension-dominated to shear-dominated behavior. Three-dimensional fracture morphology analysis further reveals that temperature and confining-axial pressure jointly regulate the fluctuation height and spatial complexity of fracture surfaces, with specimens pre-treated at a higher temperature exhibiting peak fracture surface roughness. The research results provide critical experimental evidence for optimizing parameters under coupled temperature-stress conditions in the hydraulic fracturing design of deep carbonate geothermal reservoirs.

1. Introduction

Amid the profound global energy restructuring and growing demand for clean energy, the search for low-carbon, renewable, and stable alternative energy sources has intensified. Their development has become a strategic priority for worldwide technological and economic advancement. Geothermal energy, as an abundant, stable, and nearly zero-carbon emission energy source stored within the Earth, plays a crucial role in this transition and has garnered widespread attention globally (Nkinyam et al., 2025). The Xiongan New Area in China and the North China Basin where it is located are key regions rich in geothermal resources, hosting deep Meso-

Yandy Scientific Press

*Corresponding author.
E-mail address: pengli@ustb.edu.cn (P. Li); tangchenyu0423@163.com (C. Tang); wuxinghui92@163.com (X. Wu); liuyanrock0721@163.com (Y. Liu); caimeifeng@ustb.edu.cn (M. Cai); mgorjian@eoas.ubc.ca (M. Gorjian).

Received December 29, 2025; revised January 26, 2026; accepted February 17, 2026; available online February 20, 2026.

proterozoic carbonate thermal reservoirs represented by the Gaoyuzhuang Formation of the Jixian System (Ma et al., 2022; Zhu et al., 2023). This formation is characterized by its great burial depth, often exceeding 3,000 m, and high temperature. These features make it an ideal target for enhanced geothermal systems (EGS) development. However, some deep carbonate thermal reservoirs also face challenges such as inherently low permeability, strong heterogeneity, and complex *in-situ* stress conditions (Li et al., 2024; Wu et al., 2025b). Hydraulic fracturing (HF) is a key technology for achieving "engineered reservoir creation" in such formations (Matsunaga et al., 1993; Liu et al., 2014; Jia et al., 2024). It aims to form a complex fracture network with high flow conductivity and long-term stability under deep "three-highs and one-low" conditions (i.e., high temperature, high reservoir pressure, high *in-situ* stress, and low permeability). This enhances fluid circulation and heat exchange efficiency, thereby enabling economical and efficient heat extraction. This approach eliminates the dependence of traditional geothermal systems on specific hydrogeological conditions, allowing the utilization of vast deep geothermal resources worldwide.

Against this technological backdrop, a long-overlooked yet critical scientific issue has increasingly come to the forefront. Deep, low-permeability carbonate reservoirs exist within a specific geothermal field long before drilling and fracturing fluid injection. During engineering operations, intense thermal exchange occurs between the injected low-temperature fluid and the high-temperature rock mass (Zhang and Zhao, 2019). This thermal effect is not merely a passive background condition but an active, powerful driving factor that fundamentally alters the physical and mechanical properties and fracture behavior of the rock. Traditional HF theories and design models, largely based on the mechanical response of rock at or near ambient temperature, fail to adequately account for thermo-hydro-mechanical coupling (Zhao et al., 2015; Qin et al., 2021; Yi et al., 2024; Wu et al., 2025a). Specifically for carbonate rocks, whose primary mineral components (e.g., calcite and dolomite) exhibit significant thermal sensitivity, the physico-chemical-mechanical response mechanisms under thermal cycling are particularly complex. High-temperature pre-treatment, which simulates *in-situ* reservoir temperature or temperature changes induced by thermal fluid cycling. It does not represent the instantaneous thermo-elastic shock during fluid injection. This treatment can trigger the initiation, propagation, and interconnection of microcracks through mechanisms such as anisotropic thermal expansion, grain boundary weakening, and thermal cracking. Consequently, it significantly alters the rock's pore structure, mechanical strength, deformation characteristics, and failure modes. This "initial thermal damage" state profoundly influences subsequent HF processes, including fracture initiation, propagation paths, morphological complexity, and the final fracture network structure.

In recent years, extensive research has been conducted on the HF behaviors of various rock types through theoretical analysis, laboratory experiments, and numerical simulations, achieving fruitful progress across several thematic areas. Foundational contributions to HF theory established early fracture pressure criteria based on the rock's ultimate tensile strength, emphasizing that fracturing fluid permeation alters the internal effective stress and consequently influences fracture initiation and damage processes (Hubbert and Willis, 1957). Subsequent theoretical advancements introduced the concept of unsteady hydraulic fracture propagation, suggesting that this mechanism can induce shear failure in rocks (Daneshy, 2003). Regarding the influence of fracturing fluid and injection conditions, investigations have revealed how fluid viscosity affects HF mechanisms (Ishida et al., 2004), while more recent studies have examined the coupled effects of confining pressure and injection volume on the breakdown pressure and permeability of granite during HF (Zhang et al., 2023). In the realm of temperature effects and thermal damage, systematic studies have elucidated the influence of reservoir depth, temperature, and rock heterogeneity on the fracturing behavior of granite, also considering the effects of rock microstructure on fracture propagation (Kumari et al., 2018). This line of inquiry has been extended by comparing the fracture surface morphology and heat transfer characteristics of heat-treated granite subjected to cyclic versus conventional HF (Dai et al., 2024). Moreover, the controlling role of *in-situ* stress has been extensively addressed, with research systematically summarizing how the minimum horizontal principal stress constrains fracture orientation (Zhang et al., 2018). Further investigations have demonstrated that, under different confining pressures, fractures in granite tend to become more complex under high confinement, accompanied by a significantly increased breakdown pressure (Wang et al., 2022). Advanced numerical simulations employing fully coupled three-dimensional (3D) finite element models have captured hydraulic fracture propagation in layered rocks and their interaction with bedding planes, providing valuable insights into stress-controlled fracture behavior (Wang et al., 2024). In addition, specific investigations on carbonate reservoirs have attributed the formation of complex fracture networks to interactions between hydraulic and natural fractures (Martyushev et al., 2024), while experimental studies have examined hydraulic fracture propagation and acoustic emission (AE) responses in fractured-vuggy carbonate reservoirs (Yang et al., 2024). Despite these valuable contributions, knowledge of HF under deep geothermal conditions remains limited to date because of complex *in-situ* stresses, high-temperature conditions, and formation heterogeneity (Chen et al., 2018; Zhang and Zhao, 2019; Wang et al., 2023; Song et al., 2024). Moreover, most existing research has predominantly focused on granite (as a classical representative of hot dry rock) or conventional shales and sandstones (Gale et al., 2014; Gonçalves da Silva and Einstein, 2018; He et al., 2022). Insufficient attention has been paid to low-permeability carbonate rocks, which are widely distributed in sedimentary basin geothermal systems. Experimental investigations have largely examined the individual effects of temperature or confining pressure in isolation. Consequently, systematic experimental data on the HF response of rocks under various confining pressure after different temperature pre-treatments remain scarce. Additionally, the competitive and synergistic mechanisms between temperature-induced damage and confining pressure constraints are poorly understood. Tem-

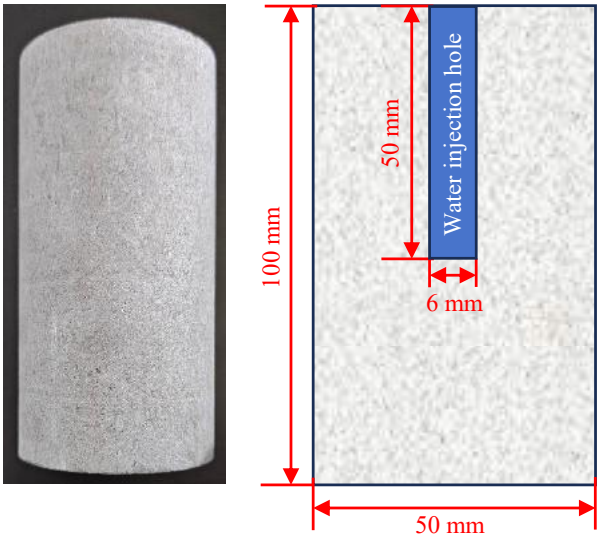

Fig. 1. The carbonate rock and the structure of the processed sample.

perature-induced damage tends to promote complex fracturing. Confining pressure may suppress propagation while also promoting shear failure, and these interactions are critical determinants of the final HF behavior. Thus, an in-depth investigation into the mechanical responses and fracture behaviors of low-permeability carbonate rocks subjected to different temperature pre-treatments under varying stress conditions during HF is of significant theoretical importance and engineering value. Such research is essential for optimizing geothermal reservoir fracturing design and enhancing geothermal extraction efficiency.

In this context, the present study focuses on low-permeability carbonate rocks from the Gaoyuzhuang Formation in Xiongan New Area of China. Utilizing a triaxial HF experimental system, tests were conducted on standard cylindrical specimens with a central borehole. The specimens were pre-heat-treated at different temperatures (20, 70, 120, 170, and 220 °C) and tested under various equivalent confining-axial pressure combinations (10, 20, 30, and 40 MPa). Note that this experiment tests the residual mechanical properties of thermally damaged rocks. It does not simulate the real-time thermal shock that occurs when cold fluid is injected into hot rock (a standard scenario in EGS), which generates immediate tensile hoop stresses. During the tests, injection pressure and AE signals were monitored and recorded in real time with high accuracy. Following the fracturing experiments, high-precision, non-contact 3D morphological scanning was employed to digitally reconstruct the resulting macroscopic fracture surfaces. By integrating fluid pressure monitoring, AE signal acquisition, and 3D fracture morphology scanning, the coupled effects of pre-treatment temperature and stress on fracture pressure, fracture propagation paths, and failure modes were systematically analyzed. Furthermore, the hydraulic fracture mechanisms of carbonate rocks under the combined influence of pre-treatment temperature and stress were revealed. The results provide critical theoretical foundations and data support for establishing HF design and prediction models suitable for deep low-permeability carbonate geothermal reservoirs.

2. Experimental methodology

2.1 Rock material and sample preparation

The carbonate rock specimens used in this experiment were collected from the Gaoyuzhuang Formation carbonate strata in Xiongan New Area of China. This formation, a key Mesoproterozoic sedimentary unit in North China, consists mainly of thick-layered limestone and dolostone with good stratification and relatively stable lithological properties. It is therefore considered one of the primary target formations for deep geothermal resource exploration and development in northern China. To minimize the impact of material heterogeneity on the experimental results, all samples were taken from the same rock block. This ensured consistent mineral composition, structural fabric, and diagenetic background, effectively controlling for experimental deviations caused by inherent differences. The rock is grayish-white with a uniform and dense texture, occasionally displaying dark spots from organic matter or fine sulfide inclusions. It possesses an intact structure without significant macroscopic fractures or dissolution pores. Measured physical parameters indicate a density range of 2,677-2,692 kg/m^3, a permeability of 2.51×10^{-20} m^2 (reflecting an ultra-low permeability), and a Mohs hardness of 3.5. These values suggest that the limestone matrix is relatively hard yet still drillable. Consequently, this rock type represents a typical reservoir rock suitable for EGS and HF applications (Alameedy et al., 2023). In addition, X-ray diffraction analysis performed on crushed carbonate samples revealed that calcium carbonate is the predominant mineral phase, with minor quantities of silicon dioxide.

Specimen preparation strictly followed the recommended standards of the International Society for Rock Mechanics. Cylindrical cores were first precisely cut using a diamond saw to produce standard specimens measuring 50 mm in diameter and 100 mm in height. To evaluate and select samples with homogeneous internal structures, each specimen underwent P-wave velocity measurement using an ultrasonic tester after cutting.

Specimens exhibiting abnormally high or low wave velocities were discarded to mitigate the potential influence of internal micro-fractures or uneven mineral distribution on the experimental outcomes. Subsequently, to simulate the fluid injection path during HF, a water injection hole with a diameter of 6 mm and a depth of 50 mm was drilled along the central axis of each specimen to serve as the initial fracture initiation channel. The specific borehole layout is illustrated in Fig. 1. After shaping, both end faces of the specimens were precision-polished to ensure that the flatness and perpendicularity deviations were strictly controlled within 0.02 mm, thereby meeting the accuracy requirements for contact surfaces in axial loading experiments. Finally, the specimens were placed in a constant-temperature oven at 60 °C for 48 h of continuous drying to thoroughly remove adsorbed water and part of the bound water, thereby eliminating the potential effects of moisture on the mechanical and thermophysical properties of the rock.

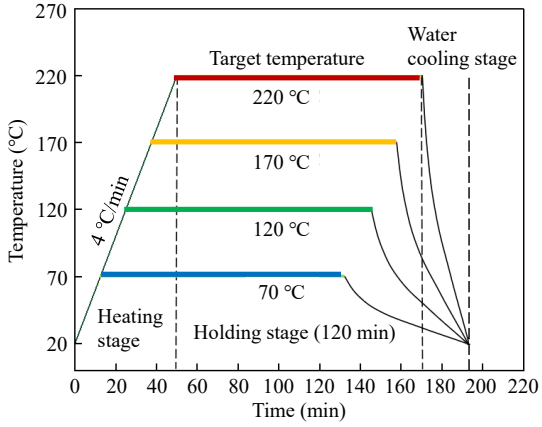

Fig. 2. The heating profiles showing temperature variation during thermal treatment at different target temperatures.

2.2 High-temperature heat treatment of the specimen

This experiment employed a programmable temperature-controlled muffle furnace to conduct systematic high-temperature thermal treatment on the prepared carbonate rock specimens. The heating device utilizes resistance wires as its core heating elements and is equipped with a multi-zone independent temperature control system. This enables uniform and stable control of the temperature field within the furnace chamber, achieving a temperature control accuracy of ±1 °C and an adjustable heating rate of 0.1-20 °C/min to meet the precise requirements of different thermal regimes. During the experiment, the specimens were placed precisely in the geometric center of the furnace chamber. This ensured uniform heating and to avoid localized overheating or thermal stress concentration caused by temperature gradients. The heating program raised the temperature from ambient to preset levels (70, 120, 170, and 220 °C, respectively) at a constant rate of 4 °C/min, followed by a 2 h holding period at each target temperature to ensure sufficient heat conduction and achieve overall temperature equilibrium. The specific temperature-time curve is illustrated in Fig. 2. Upon completion of the thermal treatment, the specimens were rapidly quenched in room-temperature water (approximately 20 °C). This rapid cooling procedure is designed to accentuate thermally induced microcracking by generating high thermal gradients, thereby simulates an extreme end-member scenario of thermal shock that could occur during rapid cold fluid injection or well shut-in/flowback events in EGS. It provides insight into the maximum potential thermal damage and its subsequent effects on mechanical properties. Moreover, this pre-treatment and subsequent cooling simulate a heating and cooling cycle that the rock might experience in a geothermal reservoir, allowing for investigation of the residual mechanical properties of thermally conditioned rock prior to fracturing.

2.3 HF experiments

To systematically investigate the mechanical behavior of HF in high-temperature pre-treated carbonate rocks under different *in-situ* stress conditions, the experiments were conducted under quasi-triaxial loading. The pressure loading system, jointly controlled by a triaxial cell and a high-pressure water pump, first applied predetermined axial pressures (10, 20, 30, and 40 MPa, respectively) to the specimens. Subsequently, fracturing fluid was injected into the pre-drilled water injection holes through the high-pressure pipeline and clamping system while corresponding confining pressures (also 10, 20, 30, and 40 MPa) were simultaneously applied. The axial and confining pressures were always maintained at equal values throughout the test to simulate a uniform *in-situ* stress field ($\sigma_1 = \sigma_2 = \sigma_3$). After the axial and confining pressures stabilized, the high-pressure pump was activated to perform HF in a constant-flow mode. Fracturing fluid was continuously injected at a rate of 5 mL/min to control the fracture initiation and propagation process, avoiding the random generation of initial fractures due to sudden pressure changes. Injection continued until macroscopic rupture of the specimen occurred. Throughout the fracturing process, high-precision pressure sensors (accuracy: 0.01 MPa) monitored and recorded the dynamic changes in the injection pore pressure in real time. This provided accurate data for analyzing fracture propagation mechanisms and breakdown pressure characteristics. In addition, red ink was utilized as a tracer by mixing it with water at a specific ratio. This colored water was injected into the pore pressure system through the high-pressure pipeline holder into the confining-axial pressure vessel. This enabled the examination of stained areas on the fracture surfaces after testing, facilitating the characterization of fracture initiation features and crack propagation patterns in the carbonate rocks. It should be noted that the equal confining-axial pressure condition creates a hydrostatic stress state ($\sigma_1 = \sigma_2 = \sigma_3$). While this simplifies the stress field to focus on the coupling effects of pre-treatment temperature and pressure on breakdown pressure and fracture complexity, it differs from field conditions where a deviatoric stress ($\sigma_v \neq \sigma_h$) governs fracture orientation. The present study provides foundational data on the hydraulic response of carbonate rocks under the coupled thermal effect and mechanical loading. For clarity, all specimens are labeled according to their pre-treatment temperature and confining-axial pressure. For example, specimen S-120-30 denotes a sample pre-treated at 120 °C and tested under a confining-axial pressure of 30 MPa.

During the HF experiments, a high-precision AE monitoring system was employed to capture the elastic wave signals released during rock fracture processes. Two AE sensors were fixed to the left and right ends of the external surface of the confining pressure chamber in the HF equipment. To ensure optimal acoustic coupling between the specimen and the sensors, a layer of Vaseline was applied to the contact interfaces. The sensors were then securely fastened using wide rubber bands and adhesive tape. The AE system was equipped with wideband sensors. The AE signal threshold was set at 40 dB, and AE events were continuously recorded at a sampling rate of 1 MHz, ensuring accurate identification of the complete evolutionary characteristics of micro-fracture initiation, propagation, and coalescence. Notably, to effectively mitigate interference from frictional noise at the interface between the inner wall of the confining pressure chamber and

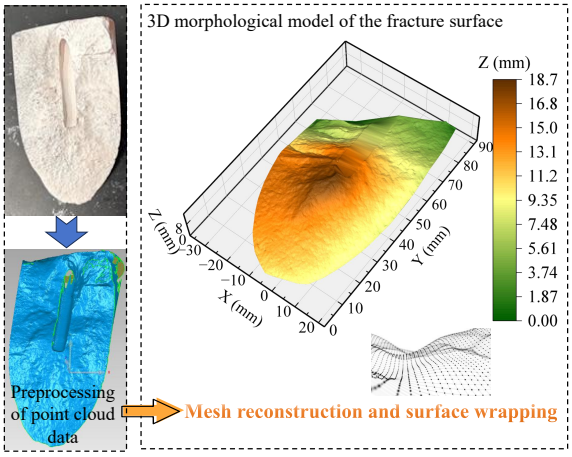

Fig. 3. Workflow of 3D fracture surface scanning and modeling.

the specimen surface, an appropriate amount of Vaseline was applied. This achieved satisfactory monitoring results. Moreover, to guarantee precise correspondence of the multi-source data, the AE acquisition system was strictly synchronized in time with the HF control system. This enabled precise correlation of each AE event with specific fracturing parameters, establishing a reliable pressure-time-AE event relationship for subsequent analysis.

2.4 3D fracture scanning

To quantitatively characterize the 3D spatial morphology of the fracture surfaces in carbonate rock specimens after HF experiments, a high-precision, OKIO-H-200 non-contact 3D profilometer was employed to perform digital modeling of typical fracture surfaces and to extract key geometric parameters. The instrument operates on the principle of structured light 3D scanning, comprising a high-precision digital grating projection device and two high-resolution industrial cameras. It achieves a resolution of 0.01 mm for high-fidelity morphology capture. During operation, the projector casts encoded grating stripes onto the fracture surface, while the dual industrial cameras synchronously capture the distorted stripe patterns modulated by the surface topography. The 3D coordinates of points on the fracture surface are then precisely calculated via triangulation based on the grating deformations, ultimately generating a dense point cloud model (Fig. 3).

3. Results

3.1 Evolution of fluid pressure over time

The complete evolution curves of internal fluid pressure versus time during HF tests performed on carbonate rock specimens are presented in Fig. 4. The confining-axial pressure level systematically controls the morphological characteristics, evolutionary paths, and key mechanical parameters of the fluid pressure curves during fracturing. These parameters include the peak breakdown pressure magnitude, the pressure increase rate during linear loading, and the duration of the nonlinear deformation phase.

Under different pre-treatment temperature conditions, the influence of confining-axial pressure on the HF process demonstrates highly consistent evolutionary patterns. As the confining-axial pressure increases from 10 to 40 MPa, the time required for the fluid pressure curve to reach its peak gradually increases. This manifests as a characteristic rightward shift of the peak. This trend is consistently observed across specimens subjected to different temperature pre-treatments. The entire fracturing process duration is significantly extended particularly under the 40 MPa high confining-axial pressure condition. This indicates that the high confining-axial pressure state effectively enhances the structural constraint capacity of the rock. It also suppresses the initiation and coalescence of microcracks, and delays the formation and propagation of main fractures. Simultaneously, the increase in confining-axial pressure markedly alters the post-failure pressure drop behavior. Under lower confining-axial pressures, such as 10 and 20 MPa, the fluid pressure curve shows an abrupt drop after the peak, reflecting the characteristics of sudden fracture propagation and brittle failure. In contrast, under higher confining-axial pressures of 30 and 40 MPa, the pressure decline after the peak becomes more gradual, demonstrating a progressive fracture propagation mode. This difference may be attributed to the increased complexity of the fracture propagation path under high confining-axial pressure. Pre-existing fractures tend to close under high pressure, and new fractures must overcome greater frictional resistance along more tortuous propagation paths. Consequently, fluid pressure dissipates more slowly.

The complete evolution curves of bottom-hole fluid pressure versus time during HF tests performed on carbonate rock specimens are shown in Fig. 5. Overall, while the fracture processes observed in all specimens during HF were highly nonlinear, the changing trends of the fluid pressure-time curves remained relatively similar. However, the pre-treatment temperature significantly influenced the fluid pressure curves. Under different confining-axial pressure conditions, the influence of temperature on rock fracturing behavior exhibited regular variations. At the lower confining-axial pressure of 10 MPa, as the pre-treatment temperature increased from 20 to 220 °C, the peak values of the fluid pressure curves changed distinctly. They exhibited a non-monotonic evolution, initially rising and then declining. It is noteworthy that as the confining-axial pressure level increases (from 20 to 40 MPa), the influence of pre-treatment temperature on the specimen breakdown pressure gradually weakens. This indicates that enhanced confining-axial pressure effectively suppresses the opening and propagation of thermally induced cracks, partially counteracting the deterioration effects caused by high-temperature pre-treatment. This phenomenon reveals the interactive relationship between temperature and stress conditions in controlling rock fracturing behavior. It provides important experimental evidence for a deeper understanding of the fracturing mechanisms of carbonate reservoirs under thermo-mechanical coupling environments. These findings can guide the optimization of reservoir stimulation design in geothermal energy development. They suggest that fracturing parameters should be selected based on actual reservoir temperature and *in-situ* stress conditions to achieve optimal permeability enhancement.

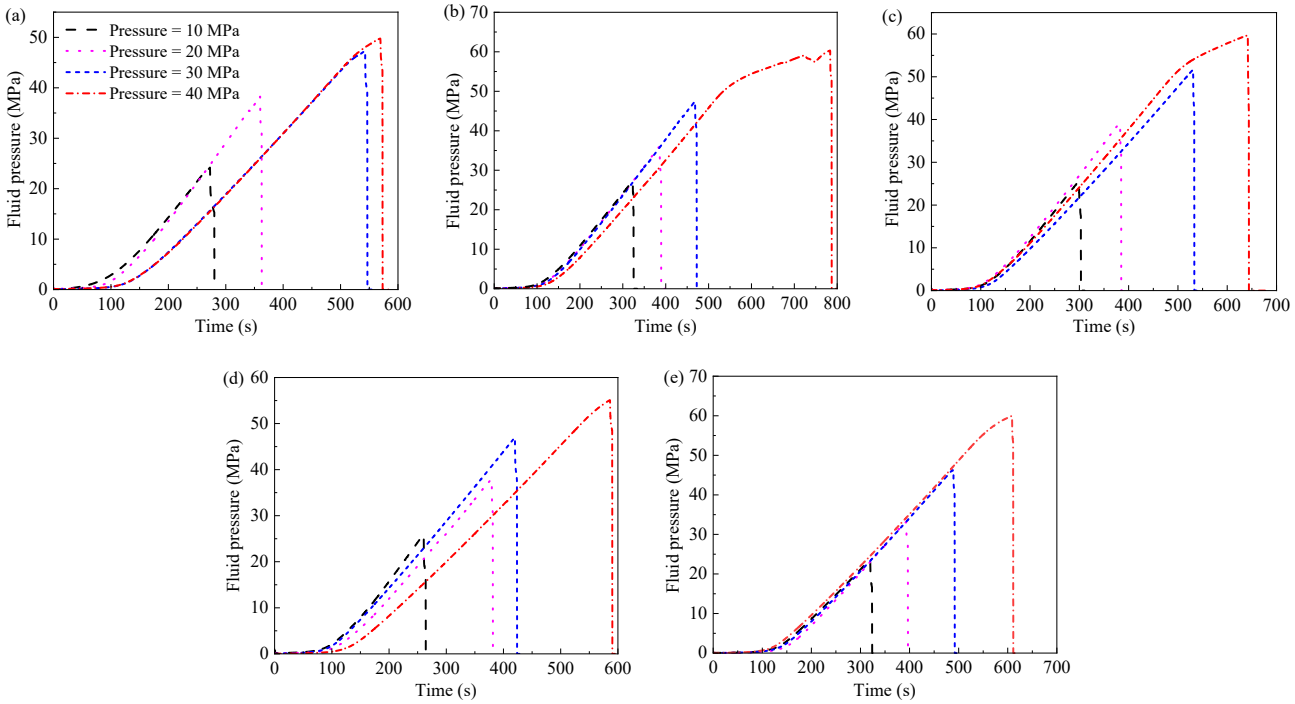

Fig. 4. Fluid pressure curves versus time during HF of the specimens under varying confining-axial pressures and subjected to the pre-treatment temperatures of (a) 20 °C, (b) 70 °C, (c) 120 °C, (d) 170 °C, and (e) 220 °C.

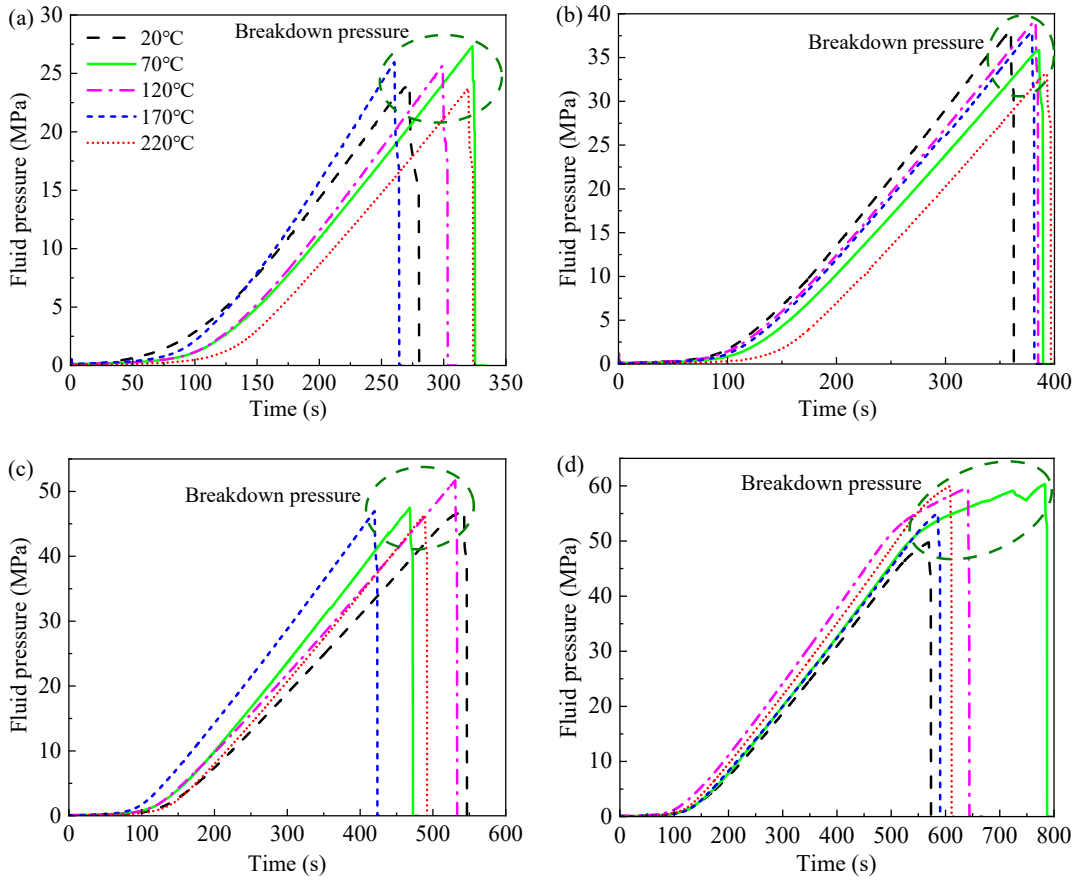

Fig. 5. Fluid pressure curves versus time during HF of the samples subjected to different pre-treatment temperatures under the confining-axial pressures of (a) 10 MPa, (b) 20 MPa, (c) 30 MPa, and (d) 40 MPa.

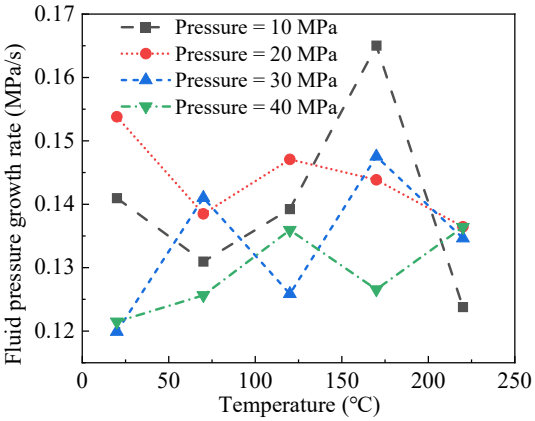

Fig. 6. Variations in fluid pressure growth rates of the samples under different confining-axial pressures with the pre-treatment temperature.

3.2 Characteristic parameter analysis

3.2.1 Growth rate of fluid pressure

The fluid pressure growth rate during the linear pressurization phase of the fluid pressure-time curve serves as a key indicator characterizing the mechanical behavior of the rock mass during HF. It directly reflects the dynamic response of the rock to injected fluid pressure under different temperature-pressure coupling conditions. This parameter essentially embodies the overall stiffness of the internal structure and the sealing integrity of the reservoir rock system before critical failure. It directly determines the accumulation efficiency of fluid energy during the fracturing process. As shown in Fig. 6, under different confining-axial pressure conditions, the fluid pressure growth rate exhibits significant nonlinear variations with pre-treatment temperature. This indicates that the parameter is synergistically regulated by temperature and confining-axial pressure, and its variation pattern exceeds the simple additive effects of individual factors.

Detailed analysis of the data trend under the 10 MPa condition reveals a clear pattern. As the treatment temperature increases from 20 to 170 °C, the slope of the linear pressurization phase continuously rises from its initial value to a peak of 0.16504 MPa/s, representing an increase of 17.02%. This demonstrates the enhancing effect of low-to-medium temperature thermal treatment on the mechanical properties of the rock. However, when the temperature further rises to 220 °C, the slope decreases sharply to 0.1238 MPa/s, a reduction of 24.85%. This indicates significant deterioration of the rock's mechanical properties under high-temperature conditions. Notably, this pattern of an initial increase followed by a decrease is also observed under other confining-axial pressure conditions, but the magnitude of change diminishes with increasing confining-axial pressure. For instance, under 30 MPa conditions, the slope reduction from 170 to 220 °C is only 8.78%, indicating that high confining-axial pressure exerts a certain inhibitory effect on high-temperature damage.

From a mechanistic perspective, this temperature-dependent variation pattern reflects the dual effects of thermal treatment on the rock's microstructure. Within the low-to-medium temperature range of 20-120/170 °C, thermal action promotes enhanced cementation between mineral particles and the closure of pre-existing micro-fractures, thereby improving the structural integrity and load-bearing capacity of the rock. This consequently increases its fluid pressure response efficiency. In contrast, when the temperature exceeds 120/170 °C, differences in thermal expansion among the various mineral components lead to thermal stress concentration. The stress concentration induces new micro-fracture networks and propagates existing defects. This weakens the intergranular bonding and the overall framework strength, ultimately resulting in reduced system sealing integrity and diminished energy accumulation capacity.

It is particularly noteworthy that under all confining-axial pressure conditions, the pressure growth rates of specimens treated at 120/170 °C reach or approach peak values. This indicates that this temperature range may represent the "optimal stiffness temperature threshold" for this type of carbonate rock. Near this temperature, the rock's internal structure achieves an optimal balance under the combined effects of thermal treatment and confining-axial pressure constraints. The micro-fracture system attains an ideal closure state that maintains sufficient structural integrity without significant thermal damage, thereby exhibiting the highest fluid pressure response efficiency. Conversely, the consistently low slope values of specimens treated at 220 °C confirm substantial degradation of rock mechanical properties under high-temperature conditions. The development of micro-fracture networks leads to "early pressure release" phenomena, allowing fluid to escape through micro-fracture channels before reaching the critical breakdown pressure. These findings not only elucidate the influence mechanism of temperature on the hydraulic stiffness of carbonate rocks but, more importantly, establish a quantitative evaluation methodology for the fluid pressure response efficiency of rocks under temperature-pressure coupling conditions. For deep geothermal reservoir stimulation engineering, these discoveries provide crucial theoretical foundations for optimizing fracturing design.

3.2.2 Breakdown pressure

The variation of breakdown pressure with pre-treatment temperature for specimens under different confining-axial pressures is plotted in Fig. 7. The results show an overall non-monotonic response characterized by an initial increase followed by a decrease, with differentiated fluctuation patterns across various confining-axial pressure levels. The influence of pre-treatment temperature on rock mechanical properties exhibits a characteristic three-stage "optimization-damage-repair" pattern. Specifically, the low-to-medium temperature range (20-70 °C) is dominated by structural densification; the medium-to-high temperature range (70-170 °C) shows progressively intensifying thermal damage effects; and the high-temperature range (170-220 °C) may exhibit partial recovery phenomena. Confining-axial pressure plays a crucial regulatory role throughout this process. High confining-axial pressure conditions ($\geq$ 30 MPa) not only significantly increase the absolute value of breakdown pressure but also enhance temperature sensitivity, making the fluctuations in the struct-

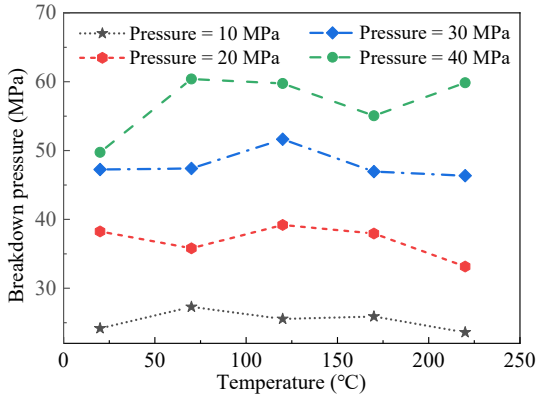

Fig. 7. Variations in breakdown pressures of the samples under different confining-axial pressures with the pre-treatment temperature.

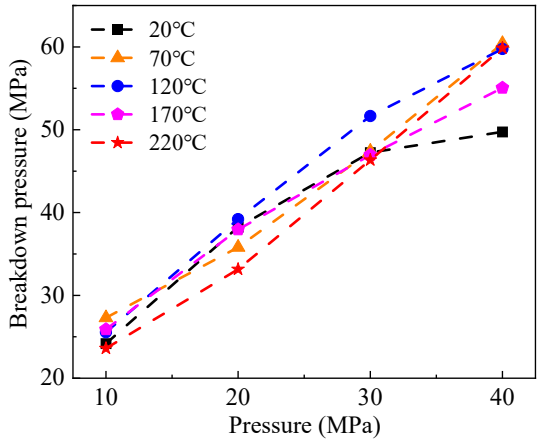

Fig. 8. Variations in breakdown pressures of the samples subjected to different pre-treatment temperatures with the confining-axial pressure.

ural damage-repair process more pronounced. In contrast, under low confining-axial pressure conditions ($\leq$ 20 MPa), high-temperature damage often exhibits irreversible characteristics with limited recovery capacity. This coupling effect of temperature and confining-axial pressure reveals the thermo-mechanical synergistic mechanisms that must be considered in deep geothermal reservoir stimulation. It provides an important theoretical basis for optimizing fracturing parameter design.

This decoupling of the temperature response by stress level provides a critical engineering design map. In deep, high-stress carbonate reservoirs, the rock may retain higher fracture initiation resistance across a wider temperature window. It may even exhibit partial recovery after high-temperature exposure. This contrasts sharply with shallow, low-stress settings where thermal damage leads to more severe and permanent strength degradation.

The evolutionary pattern of breakdown pressure in carbonate rocks with increasing confining-axial pressures (10-40 MPa) under five characteristic pre-treatment temperatures (20-220 °C) is illustrated in Fig. 8. All temperature groups demonstrate the fundamental trend of monotonically increasing breakdown pressure with rising confining-axial pressure; however, they exhibit differentiated growth patterns and sensitivity levels across the various temperature conditions.

In-depth analysis reveals that the enhancing effect of confining-axial pressure on breakdown pressure exhibits significant temperature dependence. The specimens pre-treated at 120 °C demonstrate the strongest confining-axial pressure sensitivity, maintaining consistently high growth rates of breakdown pressure across equivalent confining-axial pressure intervals (e.g., a sharp 58.3% increase occurs during the 10 to 20 MPa stage). The 220 °C high-temperature treatment group, despite having the lowest absolute breakdown pressure values, still shows a considerable increase of 27.7% during the high confining-axial pressure stage (from 30 to 40 MPa). This indicates that even severely thermally damaged rocks can achieve some degree of strength recovery through confining-axial pressure constraints. This phenomenon confirms the complexity of rock mechanical behavior under temperature-stress coupling effects. Moderate thermal treatment (120 °C) optimizes the internal rock structure and enhances its responsiveness to confining-axial pressure. In contrast, high-temperature treatment ($\geq$ 170 °C) weakens the intrinsic rock strength mainly through thermal-stress-induced microcracking and the weakening of grain boundaries or bonding materials. This makes the rock more susceptible to fracturing under equivalent confining-axial pressure conditions. These findings provide important foundational evidence for the design of HF in deep geothermal reservoirs, suggesting that operational pressure parameters should be rationally selected according to actual reservoir temperature conditions to achieve optimal stimulation outcomes.

3.3 AE characteristics during HF

AE monitoring technology provides a unique perspective for revealing the influence mechanisms of pre-treatment temperature and confining-axial pressure on the HF behavior of carbonate rocks. Under the 40 MPa condition, the AE response characteristics (including AE counts and cumulative AE energy) of carbonate rock specimens subjected to different temperature pre-treatments are shown in Fig. 9. The evolution patterns of the AE signals clearly record the entire process from micro-damage accumulation to macroscopic fracture. This provides crucial dynamic information for understanding the impact of temperature on rock fracturing behavior.

From the overall temporal characteristics, the HF process of all specimens exhibits a typical three-stage AE evolution pattern: An initial quiet period, a stable development period, and a main fracture period. During the initial fracturing stage, as fluid pressure increases linearly and steadily, AE activity generally remains in a quiet state, with only sporadic low-energy events occurring. Both cumulative AE energy and event counts maintain baseline levels. This phenomenon indicates that during this initial loading phase, no significant damage evolution has yet occurred within the internal rock structure, and the work done by the fluid pressure is primarily stored in the rock mass as elastic strain energy. It is noteworthy that the specimen S-220-40, pre-treated at 220 °C, exhibits unique AE behavior during this stage. Its cumulative AE energy shows a

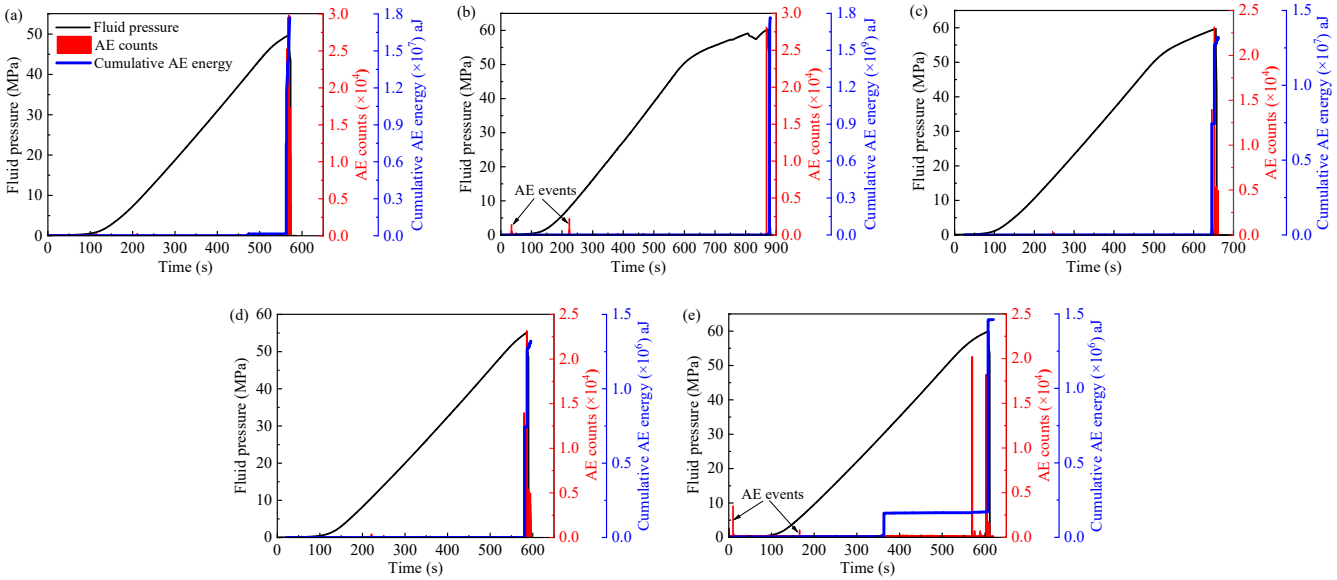

Fig. 9. Evolution process of AE counts and cumulative AE energy accompanied by the fluid pressure-time curve of the samples subjected to the pre-treatment temperatures of (a) 20 °C, (b) 70 °C, (c) 120 °C, (d) 170 °C, and (e) 220 °C under the confining-axial pressure of 40 MPa.

sustained, slight increase even during the linear pressure rise phase of fluid pressure. This anomalous signal indicates that the thermal damage caused by high-temperature pre-treatment has rendered the material metastable. As a result, pre-existing cracks begin to activate and propagate even under relatively low fluid pressure. This behavior clearly demonstrates the significant weakening effect of high-temperature pre-treatment on material stability.

When the fluid pressure approaches the peak strength (breakdown pressure) of the specimens, all samples exhibit an abrupt transition in AE activity. During this stage, the AE characteristic parameters demonstrate a burst-type growth pattern: AE counts almost instantaneously reach their peak values, while the cumulative AE energy increases by orders of magnitude. This sudden response corresponds to the formation process of macroscopic fracture surfaces in the rock, reflecting the critical transition of internal cracks from stable propagation to unstable extension.

The temperature-dependent evolution pattern of AE parameters reveals the significant influence of thermal pre-treatment on rock fracture mechanisms. The decreasing trend of AE counts with rising temperature indicates that the microcrack network induced by high-temperature pre-treatment partially "consumes" the material's damage tolerance. During subsequent HF, since part of the fracture energy has already been released during the thermal pre-treatment stage, the number of newly generated microcracks is relatively reduced, leading to a decrease in AE events during the main fracture. Particularly noteworthy is the anomalously high energy release observed in the 70 °C pre-treated specimen, which may stem from a unique coupling effect between thermal stress and mineral lattice deformation within this temperature range. Moderate thermal exposure sufficiently activates grain boundary sliding and microcrack initiation without reaching the critical state for large-scale crack interconnection. This enables the material to accumulate higher strain energy, which is then instantaneously released during final fracture. The AE responses of the 170 and 220 °C high-temperature pre-treated specimens reflect a transition in the mechanical behavior from brittle to quasi-brittle. The thermal damage induced by high temperatures not only reduces the overall strength of the material but also alters the kinetics of crack propagation. That is, it shifts from sudden, single main crack extension to the distributed, coordinated propagation of multiple cracks, thereby reducing the AE intensity at the moment of main fracture.

In carbonate rock specimens subjected to 220 °C high-temperature pre-treatment, the influence of confining-axial pressure on AE signals is shown in Fig. 10. The evolution of AE counts and cumulative AE energy clearly reflects the controlling effect of confining-axial pressure on the rock fracture mechanism, revealing a transition from simple fracture under low confining-axial pressure to complex fracture under high confining-axial pressure. Under low confining pressure (10 MPa), failure is rapid and brittle, characterized by a single, intense AE burst at breakdown. As confining-axial pressure increases, the failure process transitions from a simple, sudden event to a prolonged, staged sequence. At 40 MPa, significant AE activity emerges well before the breakdown pressure, indicating a protracted phase of microcrack adjustment and shear slip. This results in a shift from concentrated to distributed energy release; the instantaneous intensity at main fracture may decrease, but the total cumulative energy release increases substantially. The confining-axial pressure dependent variations in AE parameters reveal the crucial regulatory role of constraint stress on rock fracture mechanisms. As the confining-axial pressure increases from 10 to 40 MPa, the

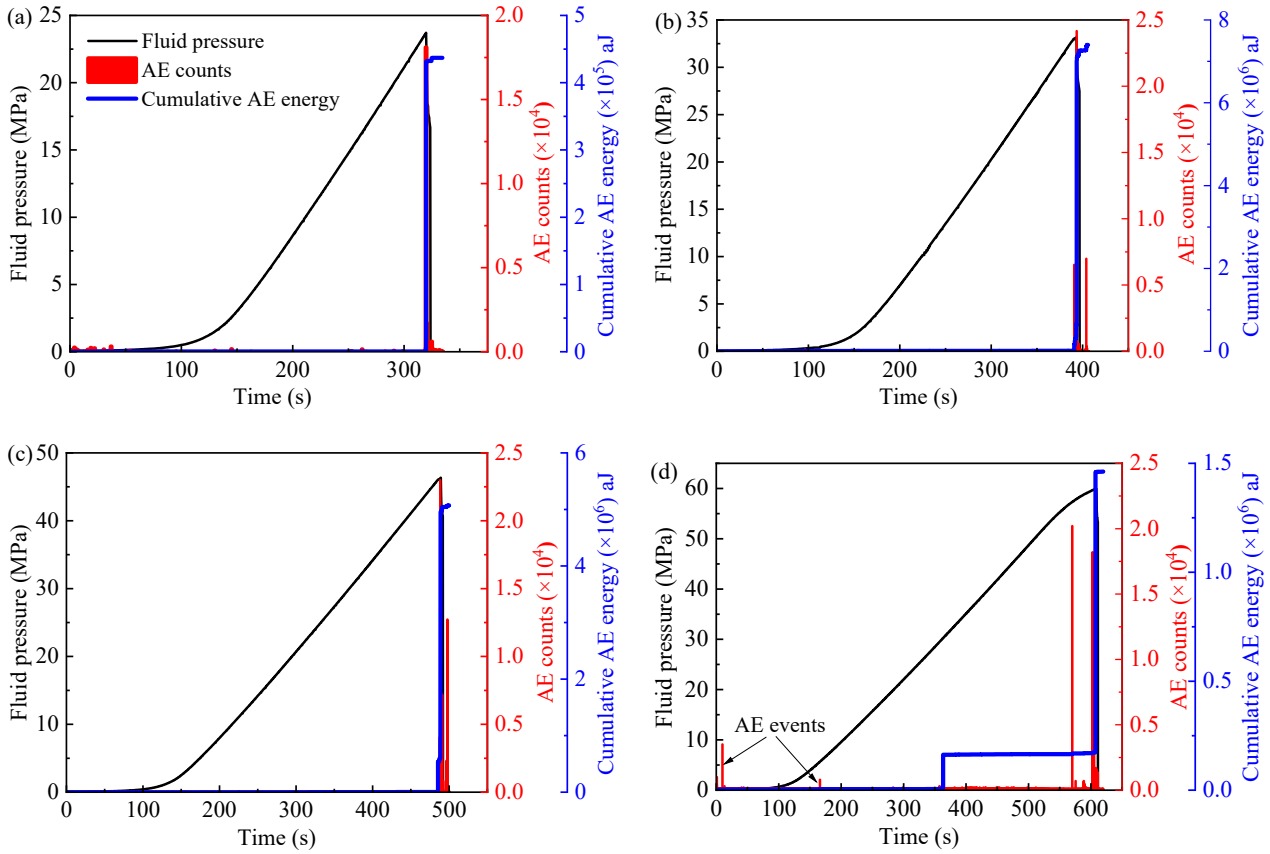

Fig. 10. Evolution process of AE counts and cumulative AE energy accompanied by the fluid pressure-time curve of the samples subjected to 220 °C under the confining-axial pressures of (a) 10, (b) 20, (c) 30, and (d) 40 MPa.

fracture mode undergoes a significant transition from tensile-dominated to shear-dominated, as will be discussed later.

This pressure-dependent AE evolution provides a diagnostic signature for the failure mode. The early, fluctuating AE signals under high confinement are precursors of shear-dominated, complex fracture propagation. For geothermal operations in high-stress, high-temperature reservoirs, this suggests that real-time AE monitoring could help identify the transition from stable damage accumulation to unstable fracture propagation, allowing for operational adjustments. Furthermore, the prolonged, energy-dispersive fracturing process under high confinement may promote the creation of a more complex and potentially more conductive fracture network, despite the higher pressures required to initiate it.

3.4 Crack propagation characteristics and failure modes

To systematically investigate the influence mechanism of temperature on fracture propagation patterns and failure modes, specimens pre-treated at different temperatures under 10 MPa confining-axial pressure were selected as representative cases for comparative analysis of failure morphology. As shown in Fig. 11, the fracture surfaces of all specimens were extensively stained with red tracer. This indicates that high-pressure fluid effectively entered and extended the pre-existing fracture systems during the fracturing process. Micro-fractures continuously coalesced and connected, ultimately forming macroscopic failure zones that led to structural instability of the rock samples. The locally unstained areas reflect an alternative failure mechanism. During high-pressure water injection, certain regions experienced compressional shear slip along fracture surfaces under fluid pressure. This shear-dominated failure mode did not establish continuously interconnected fluid pathways, consequently showing no significant staining.

Under ambient temperature conditions (20 °C), the fracture surface of sample S-20-10 penetrates the rock specimen almost vertically, exhibiting characteristic tensile failure features. This indicates that the original rock mass structure remains intact and highly isotropic; consequently, the fracture path strictly follows the direction of the maximum principal stress. As the temperature rises to 70 and 120 °C, the fracture inclination angles of samples S-70-10 and S-120-10 increase significantly. The propagation path begins to deviate from the axial stress direction, revealing a tensile-shear composite failure mode. This reflects that medium-temperature pre-treatment promotes the development of internal micro-fractures in the rock, enhances structural anisotropy, and makes fractures more prone to propagate along weak planes. When the temperature further increases to 170 and 220 °C, the fracture surfaces of the samples S-170-10 and S-220-10 transition to distinctly

Fig. 11. Crack propagation characteristics and failure modes of the samples subjected to the pre-treatment temperatures of (a) 20 °C, (b) 70 °C, (c) 120 °C, (d) 170 °C, and (e) 220 °C under the confining-axial pressure of 10 MPa.

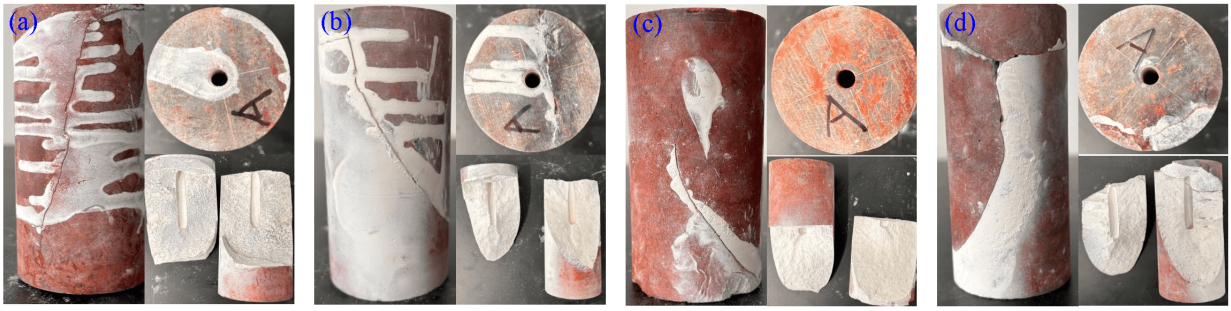

Fig. 12. Crack propagation characteristics and failure modes of the samples subjected to the pre-treatment temperature of 120 °C under the confining-axial pressures of (a) 10 MPa, (b) 20 MPa, (c) 30 MPa, and (d) 40 MPa.

oblique or even nearly horizontal distribution, with significantly increased surface roughness accompanied by evident slip traces. These morphological features indicate that shear failure completely dominates the fracture process. Particularly under the 220 °C high-temperature condition, fractures slide and connect entirely along the weakened structural planes induced by thermal treatment, demonstrating typical shear failure characteristics.

This series of morphological evolutions reveals the systematic influence of temperature on the fracture mechanism of carbonate rocks. As the pre-treatment temperature increases from 20 to 220 °C, the failure modes induced by HF undergo a complete transition sequence from tensile-dominated to tensile-shear composite, and finally to shear-dominated. The changes in the geometric characteristics of the fracture surfaces directly mirror the temperature-driven transformation of rock mechanical properties. At low-to-medium temperatures ($\leq$ 120 °C), thermal effects primarily enhance cementation between mineral particles, allowing the rock to maintain relatively high tensile strength. In contrast, high-temperature treatment ($\geq$ 170 °C) triggers extensive micro-fractures through mechanisms such as differential thermal expansion and the weakening of grain boundaries or bonding materials. This significantly reduces the rock's shear strength and shifts the failure mode toward shear dominance.

It is noteworthy that this temperature-dependent transition in failure modes is fundamentally consistent with the evolutionary patterns of previously discussed mechanical parameters (such as breakdown pressure and fluid pressure growth rate). Together, they reveal the inherent behavior characteristics of carbonate rocks during HF under thermo-mechanical coupling conditions. The research findings provide significant guidance for geothermal reservoir fracturing design. Relatively regular vertical fractures can be expected in low-temperature reservoirs, whereas the formation of complex shear fracture networks must be considered in high-temperature reservoirs, necessitating corresponding adjustments in operational parameters and monitoring schemes.

Additionally, using specimens subjected to 120 °C thermal treatment as the research subject, a systematic analysis was conducted on their failure morphology under confining-axial pressures ranging from 10 to 40 MPa. As illustrated in Fig. 12, the confining-axial pressure level exerts a decisive influence on the failure modes and fracture propagation behavior of the specimens, demonstrating distinct stress-controlled characteristics.

Under the relatively low confining-axial pressure of 10 MPa, fractures in the sample S-120-10 propagate obliquely along the axis through the entire specimen. They form a distinct main fracture surface with a wide aperture, exhibiting a typical tensile failure mode. This fracture characteristic indicates that under low constraint stress conditions, the rock's tensile strength plays a dominant role, with fractures propagating along the direction of the maximum principal stress. When the confining-axial pressure increases to 20 MPa, the fracture propagation behavior of sample S-120-20 undergoes significant changes. The fracture path shows noticeable bending, with reduced length and increased branching, presenting tensile-shear composite failure characteristics. This transition reflects that under medium confining-axial pressure conditions, the rock's shear strength begins to participate in the fracture process, inhibiting the extension of purely tensile fractures. In the higher confining-axial pressure environment of 30 MPa, fractures in sample S-120-30 further deviate from the axial

Table 1. Failure modes of carbonate rocks under different temperature pre-treatments and multi-level confining-axial pressure conditions during HF.

Pre-treatment temperature (°C)	Confining-axial pressure (MPa)			
	10	20	30	40
20	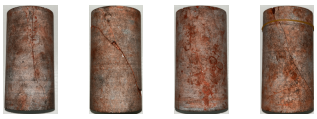			
70				
120				
170				
220	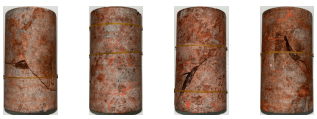			

direction. They show discontinuous and non-penetrating propagation patterns, with visible slip traces on the fracture surface. These morphological features indicate that the shear fracture mechanism has become dominant, as high confining-axial pressure effectively suppresses the development of tensile fractures, promoting failure along potential weak planes. The most significant change occurs under the high confining-axial pressure condition of 40 MPa. In the sample S-120-40, only localized short fractures form near the injection borehole, completely losing penetration capability and demonstrating typical localized shear slip failure. This phenomenon reveals the strong inhibitory effect of high confining-axial pressure on fracture propagation, transforming rock failure from overall instability to localized energy release.

From a mechanistic perspective, increasing confining-axial pressure significantly raises the energy threshold for fracture propagation by enhancing lateral constraints on the rock. This is specifically manifested in two aspects. On one hand, confining-axial pressure promotes the closure of internal micro-fractures, enhancing structural compactness and improving the overall stiffness of the rock. On the other hand, high confining-axial pressure alters the stress state of the rock, shifting the failure criterion from predominantly tensile-stress-controlled to primarily shear-stress-controlled. These findings provide important guidance for the design of HF in deep geothermal reservoirs. Specifically, well-connected main fractures can be expected in low-stress reservoirs, whereas the formation of complex fracture networks must be considered under high-stress reservoir conditions. In engineering practice, operational parameters should be optimized based on actual *in-situ* stress conditions. That is, high-flowrate fracturing should be adopted for low confining-axial pressure reservoirs, whereas elevated injection pressures and other measures are required to overcome the inhibitory effect of *in-situ* stress on fracture propagation in high confining-axial pressure reservoirs.

The failure modes of HF in carbonate rocks under different temperature pre-treatment conditions and multi-level confining-axial pressure conditions are systematically summarized in Table 1. The results demonstrate that the coupled effects of temperature and confining-axial pressure exert significant control on fracture propagation behavior, forming a complete evolutionary sequence from simple tensile fracture to complex shear failure.

In the low-temperature and low confining-axial pressure region (20 °C/10 MPa), the specimens exhibit typical axially penetrating fractures with wide apertures and smooth surfaces, demonstrating pure tensile failure mechanisms. As the temperature increases to 70, 120, and 170 °C under the same low confining-axial pressure, fractures begin to show branching and deflection, forming composite failure modes dominated by tensile failure with localized shear components. When the temperature further rises to 220 °C, even under the 10 MPa low confining-axial pressure, the fractures completely transition to shear failure through slip along weak planes. This reflects the significant weakening effect of high temperature on rock structural strength. At lower confining-axial pressure (10 MPa), obliquely penetrating fractures form. As the confining-axial pressure increases, multi-segment discontinuous propagation occurs and localized short fractures develop. At a high confining-axial pressure of 40 MPa, shear fractures become more predominant. This variation pattern confirms the strong constraining effect of confining pressure on fracture propagation. Its mechanical essence lies in the enhancement of rock shear strength by confining pressure and the alteration of the rock mass's stress state, causing the failure criterion to transition from the maximum tensile stress theory to the Coulomb-Mohr criterion.

From an engineering geology perspective, the synergistic interaction between temperature and confining pressure governs three key characteristics of the fracture system. First, fracture connectivity significantly decreases with increasing temperature and confining pressure. Second, fracture surface morphology transitions from smooth and planar to rough and faulted. Third, the failure mechanism evolves from global instability to localized damage. These regularities provide crucial guidance for geothermal reservoir stimulation. Effective interconnected fracture networks can be formed in shallow, low-temperature reservoirs. In contrast, under deep, high-temperature reservoir conditions, higher injection pressures or optimized fracturing fluid properties must be employed to overcome the suppression of fracture propagation by high *in-situ* stresses.

The temperature-stress-failure morphology correspondence established in this study provides a theoretical basis for accurately predicting reservoir stimulation outcomes under different geological conditions. It is recommended that, in practical engineering applications, appropriate fracturing process

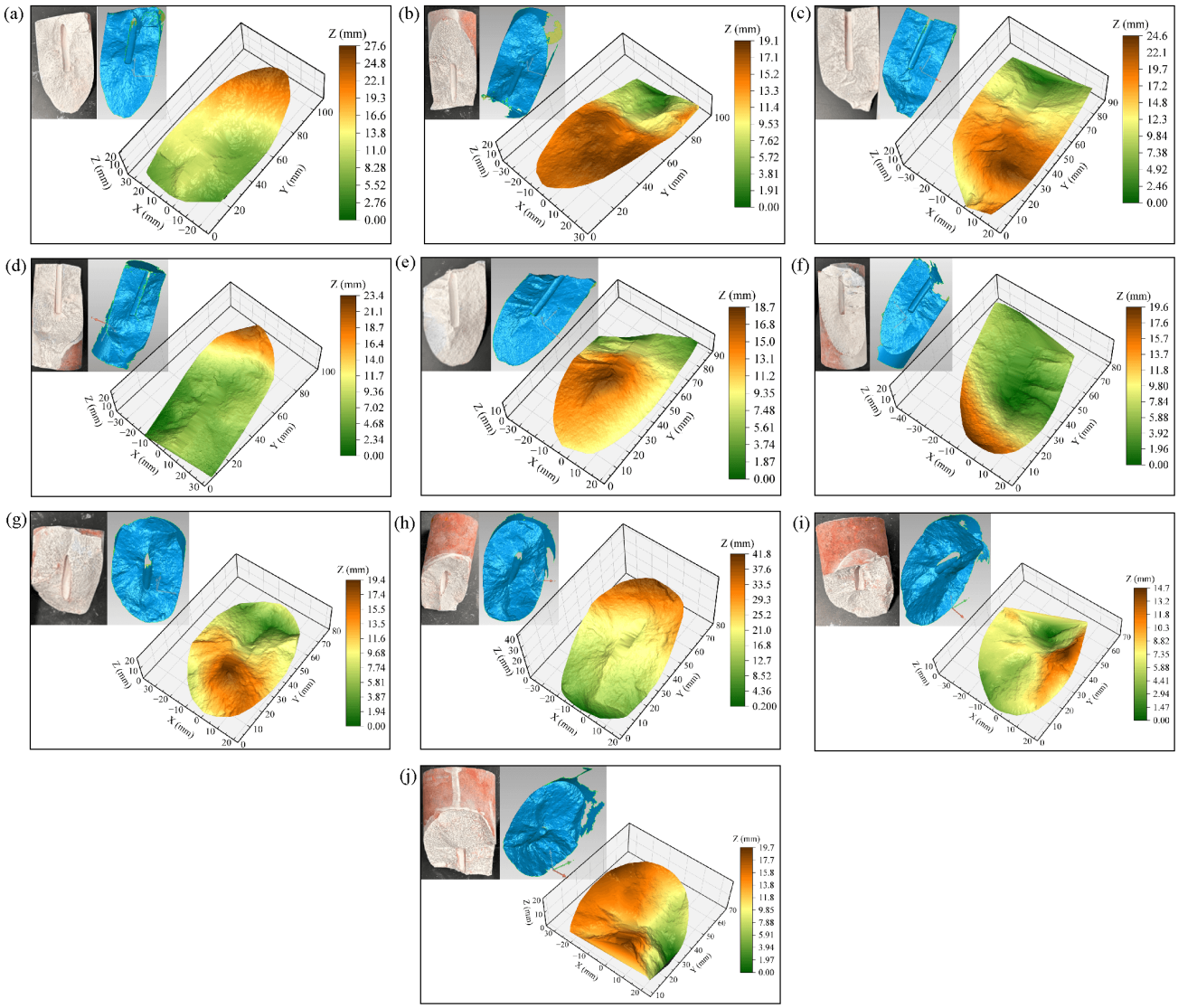

Fig. 13. 3D morphological characteristics of the specimen fracture surface A and B after the pre-treatment temperatures of (a)-(b) 20 °C, (c)-(d) 70 °C, (e)-(f) 120 °C, (g)-(h) 170 °C, and (i)-(j) 220 °C under the confining-axial pressure of 40 MPa.

parameters should be selected according to the temperature and *in-situ* stress conditions of the target formation. For high-temperature and high-stress reservoirs, complex fracture network construction technologies such as multi-stage injection and temporary plugging and diversion should be adopted. Conventional reservoirs can continue to utilize traditional single-stage fracturing processes, thereby achieving cost-effective reservoir stimulation.

3.5 3D morphology characterization

3.5.1 Morphological characteristics of the fracture surfaces

The 3D point cloud models obtained through morphological scanning provide an accurate data foundation for the quantitative analysis of HF fracture surface characteristics. Their core value lies in the complete recording of elevation information for each point on the structural surface, thereby enabling the detailed characterization of the morphological heterogeneity in different directions. Taking the 40 MPa confining-axial pressure condition as an example, Fig. 13 displays the 3D morphological characteristics of the fracture surfaces of carbonate rock specimens after different temperature pre-treatments. The fracture surfaces of all specimens exhibit complex morphological structures, including multiple depressed areas and protrusions. This indicates that the fluid pressure during HF induced significant surface disturbance and structural deformation. Locally, elongated crack-like grooves are observed, corresponding to micro-fractures or secondary fracture propagation paths. The degree of undulation and the distribution density of surface protrusions on the fracture surfaces show systematic variations with pre-treatment temperature.

A systematic comparison of fracture surface morphologies at different temperatures reveals a significant evolution in the rupture mode as the pre-treatment temperature increases.

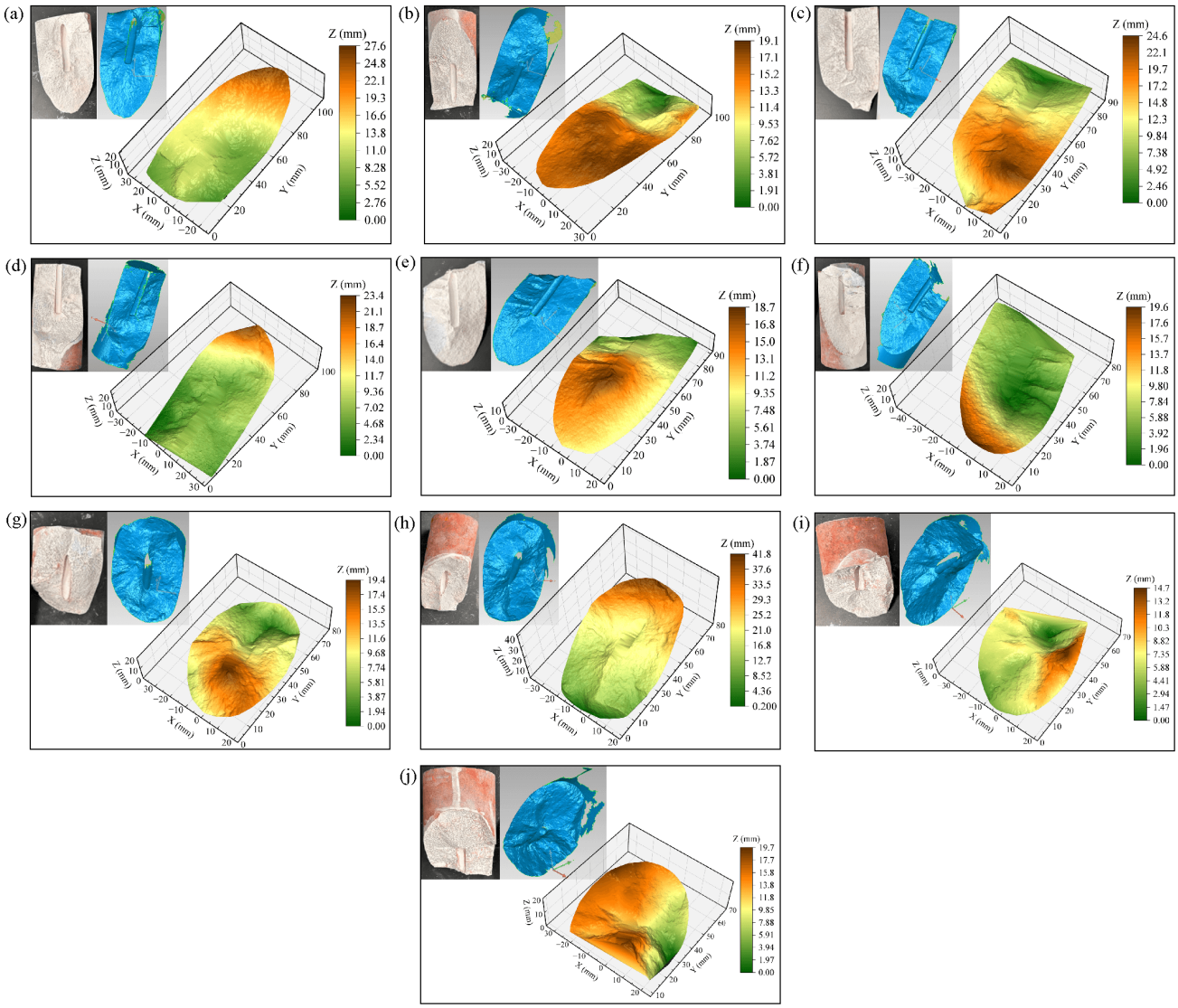

Fig. 14. 3D morphological characteristics of the specimen fracture surface A and B after 220 °C pre-treatment under the confining-axial pressures of (a)-(b) 10, (c)-(d) 20, (e)-(f) 30, and (g)-(h) 40 MPa.

The mode transitions from a concentrated tensile rupture at 20 °C to a burst-type, high-energy tensile-shear mixed-mode rupture at 70 °C. It then shifts to a diffuse multi-point rupture within the 120-170 °C range, ultimately culminating in a softened plastic rupture at 220 °C. Notably, the maximum height difference of the fracture surface peaks at 70 °C, reaching approximately 24.6 mm, and then gradually decreases with further temperature elevation. This trend suggests that moderate intermediate-temperature pre-treatment may enhance the rock's brittle behavior and energy accumulation capacity. In contrast, high-temperature conditions promote the development of thermal crack networks and the weakening of cementing materials. This leads to reduced fracture surface undulation and degraded cohesive performance, which significantly influences energy distribution during rupture and the formation of fracture paths. The morphological evolution law profoundly reveals the thermal control mechanism of temperature on the fracture behavior. It provides an important theoretical basis and design reference for optimizing HF processes in geothermal reservoirs.

To further investigate the influence of confining-axial pressure conditions on the HF behavior, the 3D morphological characteristics of fracture surfaces under different gradient confining-axial pressure after 220 °C pre-treatment were systematically analyzed, as shown in Fig. 14. A clear transition trend in the HF behavior of carbonate rocks can be identified with increasing confining-axial pressure. The failure mode evolves from a tension-dominated rough propagation mode at 10 MPa to an inhibited closed-fracture mode at 20 MPa. It then develops into a shear-slip mixed mode at 30 MPa, and ultimately forms a localized high-energy concentration rupture mode at 40 MPa. This evolutionary pattern profoundly reveals the controlling effect of confining-axial pressure conditions on fracture propagation mechanisms. Low confining-axial pressure promotes the full development and complexity of fracture networks. In contrast, high confining-axial pressure

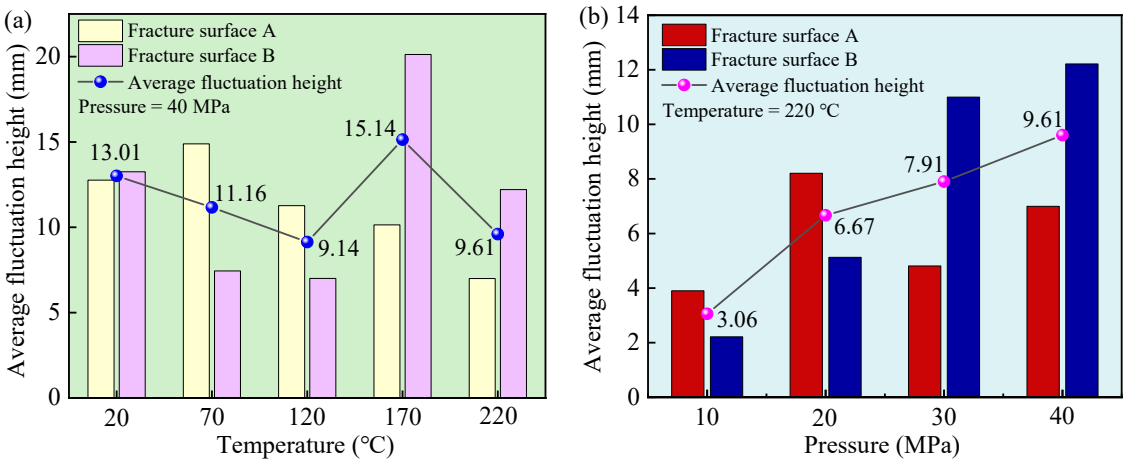

Fig. 15. Evolutionary pattern of the average fluctuation heights of the hydraulic fracture surface A and B in carbonate rock specimens with (a) pre-treatment temperature and (b) confining-axial pressure.

enhances the rock's constraint effect and alters its stress distribution states, consequently influencing both the fracture propagation paths and energy release modes. The research findings provide significant guidance for fracturing stimulation in deep geothermal reservoirs. For lower confining pressure reservoirs, large-displacement fracturing can be employed to create complex fracture networks. In contrast, high confining pressure reservoirs require optimized perforation orientation and fracturing parameters to achieve effective localized rupture control.

3.5.2 Fracture surface fluctuation height characteristics

The average fluctuation height of the fracture surface, defined as the mean value of the fluctuation heights of fracture surfaces A and B, serves as a fundamental 3D morphological parameter for quantifying roughness and unevenness. It provides a critical metric for assessing geometric complexity and directly reflects the path tortuosity and structural heterogeneity of fractures propagating through rock during HF. Under the 40 MPa condition, the evolution of the average fluctuation heights of the HF fracture surfaces in carbonate rock specimens after different temperature pre-treatments is shown in Fig. 15(a). Under the 20 °C condition, both fracture surfaces A and B maintained relatively high fluctuation states, with an average fluctuation height of 13.01 mm. This indicates that the heterogeneity of the original rock mass structure and natural defects dominated the selection of fracture paths, resulting in a relatively tortuous fracture propagation trajectory. When the temperature was raised to 70 °C, the average fluctuation height of fracture surface A slightly increased, while that of fracture surface B decreased significantly. This led to an overall average reduction to 11.16 mm. This phenomenon suggests that the low-temperature heating-water cooling cycle treatment had not yet effectively promoted internal damage accumulation. Limited thermal stress effects failed to significantly enhance the fracture surface roughness. Under the 120 °C pre-treatment condition, the fluctuation heights of fracture surfaces A and B further decreased, with the average value dropping to 9.14 mm (the lowest point in the entire temperature series). At this stage, although thermal shock had induced the initiation of some microcracks, these microcracks had not fully propagated or interconnected, resulting in an overall fracture surface tending toward a relatively flat morphology. When the temperature increased to 170 °C, the fracture surface morphology underwent significant changes. The height of fracture surface B surged sharply, and fracture surface A also showed a rebound trend, with the average fluctuation height reaching a peak of 15.14 mm. Under this temperature condition, the rock mass experienced the most pronounced accumulation of thermal stress. The intense thermal contraction effect during water cooling promoted the large-scale propagation and interconnection of microcracks, ultimately forming a fracture surface with highly rough characteristics. Under the 220 °C condition, the average fluctuation height decreased to 9.61 mm. This reduction may be attributed to the structural softening of the rock mass induced by the excessively high temperature and the enhanced plasticity of some mineral components. These changes cause the fracture propagation mode to shift from tensile-dominated failure to shear slip, accompanied by partial closure of pre-existing microcracks or slip along weak planes. This ultimately led to a significant reduction in the roughness of the formed fracture surface.

The fluctuation height of the fracture surface follows a distinct nonlinear evolution pattern with pre-treatment temperature. It reaches its minimum value at 120 °C, indicating that the thermal stress release at this temperature has not yet reached the critical state required to drive the formation of rough fractures. In contrast, it peaks at 170 °C, demonstrating that this temperature range represents the optimal window for thermal stress accumulation and release. The rock mass undergoes intense thermal expansion and water-cooling contraction cycles, leading to full development and interconnection of internal microcrack networks and ultimately forming highly undulating complex fracture surfaces. When the temperature further increases to 220 °C, the fracture propagation mechanism undergoes a fundamental change due to the softening of

the rock matrix. This results in a significant reduction in the fluctuation degree of the fracture surface. This temperature-fluctuation height evolution pattern profoundly reveals the thermal control mechanism of pre-treatment on the fracture behavior of carbonate rocks.

The evolution of average fluctuation heights for carbonate rock specimens subjected to 220 °C high-temperature pre-treatment under different confining-axial pressure conditions is illustrated in Fig. 15(b). Under the 10 MPa condition, the average fluctuation height of the specimen's fracture surface is only 3.06 mm, the minimum value among all confining-axial pressure levels. This phenomenon indicates that in a low-constraint stress environment, fractures within the rock can propagate relatively freely, forming relatively straight fracture paths, with the failure mechanism dominated by tensile failure, resulting in low fracture surface fluctuation. When the confining-axial pressure increases to 20 MPa, the average fluctuation height of the fracture surface significantly rises to 6.67 mm, an increase of approximately 118%. This change demonstrates that moderate confining-axial pressure begins to exert a noticeable constraining effect on fracture propagation, causing the fracture path to deflect and branch. This transitions the failure mode from pure tensile failure to a tensile-shear mixed mode, increasing the number of microcracks and notably enhancing the roughness and complexity of the fracture surface. Under the higher confining-axial pressure condition of 30 MPa, the average fluctuation height of the fracture surface further increases to 7.91 mm, indicating a continued strengthening of the confining-axial pressure constraint effect. At this pressure level, the rock's failure mechanism shifts further toward shear dominance. More slip and dislocation occur during fracture propagation within the confined space, forming more complex fluctuation morphologies. It is noteworthy that although the enhanced confining-axial pressure restricts the overall propagation range of the fractures, it promotes energy concentration and intense local damage. When the confining-axial pressure reaches 40 MPa, the average fluctuation height of the fracture surface peaks at 9.61 mm, an increase of approximately 214% compared to the 10 MPa condition. This result indicates that in a high confining-axial pressure environment, although the macroscopic propagation of fractures is strongly suppressed, the local stress concentration effect is significantly enhanced. This leads to intense energy release and structural damage within limited areas, ultimately forming highly undulating and complex fracture surface morphologies.

In summary, as the confining-axial pressure increases from 10 to 40 MPa, the average fluctuation height of the fracture surface exhibits a continuously rising trend. This pattern reveals the significant influence of confining-axial pressure conditions on rock fracture behavior. Under low confining-axial pressure, fracture propagation is predominantly characterized by energy-dissipative tensile failure, resulting in relatively smooth fracture surfaces. In contrast, with increasing confining-axial pressure, the fracture mechanism gradually shifts toward energy-concentrated shear failure, inducing more intense structural perturbations and morphological undulations in localized regions.

3.6 Discussion

The present study systematically reveals a non-monotonic "optimization-damage-recovery" response of breakdown pressure to temperature, a phenomenon that is less pronounced or absent in more homogeneous granite. This behavior is closely linked to the specific thermal sensitivity of calcite and the inherent fabric heterogeneity of carbonate rocks. Furthermore, while granite typically exhibits monotonic strength degradation with temperature (He et al., 2025; Li et al., 2019; Ma et al., 2023), carbonate rocks show a distinct cementation-enhancing effect at moderate temperatures (70-120 °C). They also exhibit potential for micro-crack closure under high confinement at very high temperatures (170-220 °C). Both of these characteristics are attributable to their unique grain-boundary characteristics and mineralogy. This work also identifies the existence of an "optimal stiffness-temperature window" ($\sim$ 120-170 °C) for stimulation efficiency and highlights the critical need to manage the transition toward shear-dominated, less-connected fracture networks in high-temperature carbonate reservoirs. This behavior markedly differs from the tensile-dominated, well-connected fractures typically targeted in granite-based EGS (Butt et al., 2025; Qiao et al., 2022; Tan et al., 2025). Together, these findings underscore the novelty and contribution of this research.

It is worth emphasizing that the experimental results were obtained under a simplified hydrostatic stress condition. In real geothermal reservoirs with anisotropic stress ($\sigma_1 \neq \sigma_2 \neq \sigma_3$), the minimum horizontal stress would exert a stronger directional control on fracture orientation, likely promoting planar, tensile-dominated fractures aligned with the maximum horizontal stress (Guo et al., 2021; Zhao et al., 2025). Under such conditions, the shear-enhancing effects of high temperature and confining-axial pressure observed here might be partially suppressed or manifest differently in terms of fracture tortuosity and network complexity. Future work employing true-triaxial stress states ($\sigma_1 > \sigma_2 > \sigma_3$) is recommended to directly investigate the combined effects of temperature and deviatoric stress on fracture propagation orientation and network complexity in carbonates. This would more closely simulate *in-situ* reservoir conditions. The rapid quenching protocol adopted here represents a high-cooling-rate scenario. In reservoirs where cooling is more gradual or cyclic, the extent of thermal cracking might be less severe, potentially shifting the observed temperature thresholds for strength degradation and failure mode transition. The sensitivity of carbonate fracture behavior to cooling rate warrants further investigation to better represent long-term thermal cycling conditions. Moreover, it is important to distinguish the mechanism studied here (the effect of pre-existing thermal damage on rock fracturability) from the real-time thermal shock stress induced by injecting cold fluid into hot rock. The latter generates immediate tensile hoop stresses around the borehole, which can dominate fracture initiation. The present study focuses on how prior thermal history alters the intrinsic strength and fracture propagation behavior of the rock mass itself. In addition, advanced AE parameters such as RA-AF analysis, *b*-value evolution, and frequency distribution hold

significant potential for elucidating the microscopic mechanisms of thermal cracking and failure-mode transitions in carbonate rocks. Future studies could effectively employ these analytical tools to conduct more detailed micro-mechanical investigations into thermal damage and fracture behavior.

4. Conclusions

1) Both confining-axial pressure and pre-treatment temperature significantly influence the fluid pressure evolution. Higher confining-axial pressures delay fracture initiation and alter the post-peak pressure drop behavior from brittle to progressive failure. The fluid pressure growth rate exhibits a non-monotonic response to temperature, peaking at moderate temperatures (120-170 °C) and declining sharply at 220 °C. This indicates an optimal temperature range for rock stiffness under the confining-axial pressure condition. Breakdown pressure shows a three-stage response to temperature ("optimization-damage-repair"), which is strongly modulated by the confining-axial pressure. High confining-axial pressure ($\geq$ 30 MPa) enhances both the absolute value and temperature sensitivity of breakdown pressure.
2) AE monitoring reveals that high-temperature pre-treatment ($\geq$ 170 °C) transitions the fracture mechanism from brittle to quasi-brittle, reducing AE event counts and energy release intensity. In contrast, moderate temperatures (e.g., 70 °C) can enhance energy accumulation and release.
3) Increasing the pre-treatment temperature systematically shifts the failure mode from tensile-dominated to shear-dominated. Simultaneously, increasing confining-axial pressure restricts fracture propagation and promotes localized shear slip, leading to more complex and less connected fracture networks.
4) Fracture surface morphology evolves from rough tensile fractures at low temperatures to smoother shear-dominated surfaces at high temperatures. Maximum roughness is observed at 170 °C under high confining-axial pressure. The average fluctuation height peaks at 170 °C and under high confining-axial pressure (40 MPa), reflecting intense local energy release and complex fracture paths under combined thermal and mechanical constraints.

Acknowledgements

This work was financially supported by the Science and Technology Innovation Program of Xiongan New Area (No. 2023XAGG0061) and the National Natural Science Foundation of China (Nos. 52204084 and 52474091).

Conflicts of interest

The authors declare no competing interest.

References

Alameedy, U., Fatah, A., Abbas, A. K., et al. Matrix acidizing in carbonate rocks and the impact on geomechanical properties: A review. Fuel, 2023, 349: 128586.

Butt, A., Hedayat, A., Moradian, O. Energy budgeting of laboratory hydraulic fracturing in granite with different viscosity injection fluids. Geomechanics and Geophysics for Geo-Energy and Geo-Resources, 2025, 11(1): 74.

Chen, Z., Yang, Z., Wang, M. Hydro-mechanical coupled mechanisms of hydraulic fracture propagation in rocks with cemented natural fractures. Journal of Petroleum Science and Engineering, 2018, 163: 421-434.

Dai, H., Yin, T., Wu, Y., et al. A study of geothermal hydraulic fracture surface morphology and heat transfer characteristics. Energy, 2024, 312: 133527.

Daneshy, A. A. Off-balance growth: A new concept in hydraulic fracturing. Journal of Petroleum Technology, 2003, 55(4): 78-85.

Gale, J. F. W., Laubach, S. E., Olson, J. E., et al. Natural fractures in shale: A review and new observations. AAPG Bulletin, 2014, 98(11): 2165-2216.

Gonçalves da Silva, B., Einstein, H. Physical processes involved in the laboratory hydraulic fracturing of granite: Visual observations and interpretation. Engineering Fracture Mechanics, 2018, 191: 125-142.

Guo, J., Zhan, L., Gou, B., et al. Formation of fractures in carbonate rocks by pad acid fracturing with different states of carbon dioxide. Petroleum Exploration and Development, 2021, 48(3): 744-751.

He, X., Li. P., Ning, J., et al. Geochemical processes during hydraulic fracturing in a tight sandstone reservoir revealed by field and laboratory experiments. Journal of Hydrology, 2022, 612: 128292.

He, J., Zhuang, L., Li, M., et al. Experimental and numerical analysis of hydraulic fracture propagation in naturally fractured granite cores. Geomechanics for Energy and the Environment, 2025, 43: 100695.

Hubbert, M. K., Willis, D. G. Mechanics of hydraulic fracturing. Transactions of Society of Petroleum Engineers of AIME, 1957, 210(1): 153-168.

Ishida, T., Chen, Q., Mizuta, Y., et al. Influence of fluid viscosity on the hydraulic fracturing mechanism. Journal of Energy Resources Technology, 2004, 126(3): 190-200.

Jia, L., Peng, S., Wu, B., et al. Research on quantitative characterization of 3D fractures induced by hydraulic fracturing: Insights from experimental analysis and mathematical models. Rock Mechanics and Rock Engineering, 2024, 57(3): 1997-2016.

Kumari, W. G. P., Ranjith, P. G., Perera, M. S. A., et al. Hydraulic fracturing under high temperature and pressure conditions with micro CT applications: Geothermal energy from hot dry rocks. Fuel, 2018, 230: 138-154.

Li, B., Gonçalves da Silva, B., Einstein, H. Laboratory hydraulic fracturing of granite: Acoustic emission observations and interpretation. Engineering Fracture Mechanics, 2019, 209: 200-220.

Li, P., Liu, Y., Cai, M., et al. Accurate stress measurement

using hydraulic fracturing in deep low-permeability reservoirs: Challenges and research directions. Advances in Geo-Energy Research, 2024, 14(3): 165-169.

Liu, Z., Chen, M., Zhang, G. Analysis of the influence of a natural fracture network on hydraulic fracture propagation in carbonate formations. Rock Mechanics and Rock Engineering, 2014, 47(2): 575-587.

Ma, F., Wang, G. L., Zhu, X., et al. Experimental study of the enhanced stimulation of a deep carbonate thermal reservoir in the Xiong'an New Area. Chinese Journal of Engineering, 2022, 44(10): 1789-1798. (in Chinese)

Ma, X., Wang, G., Hu, D., et al. Hydraulic fracturing of granite under real-time high temperature and true triaxial stress. Journal of Central South University, 2023, 30(1): 243-256.

Martyushev, D. A., Yang, Y., Kazemzadeh, Y., et al. Understanding the mechanism of hydraulic fracturing in naturally fractured carbonate reservoirs: Microseismic monitoring and well testing. Arabian Journal for Science and Engineering, 2024, 49(6): 8573-8586.

Matsunaga, I., Kobayashi, H., Sasaki, S., et al. Studying hydraulic fracturing mechanism by laboratory experiments with acoustic emission monitoring. International Journal of Rock Mechanics and Mining Sciences & Geomechanics Abstracts, 1993, 30(7): 909-912.

Nkinyam, C. M., Ujah, C. O., Asadu, C. O., et al. Exploring geothermal energy as a sustainable source of energy: A systemic review. Unconventional Resources, 2025, 6: 100149.

Qiao, J., Tang, X., Hu, M., et al. The hydraulic fracturing with multiple influencing factors in carbonate fracture-cavity reservoirs. Computers and Geotechnics, 2022, 147: 104773.

Qin, M., Yang, D., Chen, W., et al. Hydraulic fracturing network modeling based on peridynamics. Engineering Fracture Mechanics, 2021, 247: 107676.

Song, X., Liu, Y., Yang, X., et al. Quantifying the impact of geological and construction factors on hydraulic fracture dynamics in heterogeneous rock layers using the phase field method. Computers and Geotechnics, 2024, 169: 106223.

Tan, Z., Fu, G., Bai, T., et al. Numerical simulations of hydraulic fracturing in carbonate-type hot dry rock reservoirs based on the coupled thermo-hydraulic-mechanical-damage (THMD) model. Energy Science & Engineering, 2025, 13(12): 5821-5834.

Wang, F., Liu, W., Deng, J., et al. Hydraulic fracture propagation research in layered rocks based on 3D FEM modeling and laboratory experiments. Geoenergy Science and Engineering, 2024, 234: 212670.

Wang, H., Wang, G., Chen, Y., et al. Laboratory hydraulic fracturing of large-scale granite characterized by acoustic emission under different confining conditions. Frontiers in Earth Science, 2022, 10: 2022.

Wang, X., Li, P., Qi, T., et al. A framework to model the hydraulic fracturing with thermo-hydro-mechanical coupling based on the variational phase-field approach. Computer Methods in Applied Mechanics and Engineering, 2023, 417: 116406.

Wu, X., Cai, M., Wu, X., et al. Experimental study on nonlinear failure criterion of HDR under cyclic water-induced thermal shock. Bulletin of Engineering Geology and the Environment, 2025a, 84(5): 255.

Wu, X., Li, P., Miao, S., et al. Multi-field coupling mechanism and optimization of heat transfer in deep carbonate geothermal reservoirs based on acid fracturing modification. Case Studies in Thermal Engineering, 2025b, 73: 106591.

Yang, H., Wang, L., Bi, Z., et al. Experimental investigation into the process of hydraulic fracture propagation and the response of acoustic emissions in fracture-cavity carbonate reservoirs. Processes, 2024, 12(4): 660.

Yi, D., Yi, L., Yang, Z., et al. Coupled thermo-hydro-mechanical-phase field modelling for hydraulic fracturing in thermo-poroelastic media. Computers and Geotechnics, 2024, 166: 105949.

Zhang, W., Guo, T., Qu, Z., et al. Research of fracture initiation and propagation in HDR fracturing under thermal stress from meso-damage perspective. Energy, 2019, 178: 508-521.

Zhang, W., Xie, H., Li, M. Influences of confining pressure and injection rate on breakdown pressure and permeability in granite hydraulic fracturing. Energy Science & Engineering, 2023, 11(7): 2385-2394.

Zhang, Y., Zhao, G. A global review of deep geothermal energy exploration: From a view of rock mechanics and engineering. Geomechanics and Geophysics for Geo-Energy and Geo-Resources, 2019, 6(1): 4.

Zhang, Y., Zhang, J., Yuan, B., et al. In-situ stresses controlling hydraulic fracture propagation and fracture breakdown pressure. Journal of Petroleum Science and Engineering, 2018, 164: 164-173.

Zhao, H., Liu, Z., Yu, C., et al. Study on the propagation law of acid fracturing in cave carbonate rock. Environmental Earth Sciences, 2025, 84(8): 214.

Zhao, Y., Feng, Z., Feng, Z., et al. THM (Thermo-hydro-mechanical) coupled mathematical model of fractured media and numerical simulation of a 3D enhanced geothermal system at 573 K and buried depth 6000-7000 M. Energy, 2015, 82: 193-205.

Zhu, Y., Li, D., Hu, Y., et al. Deep structure of the Rongcheng geothermal field, Xiongan New Area: Constraints from resistivity data and boreholes. Geothermics, 2023, 114: 102776.